Robust and Adaptive Position Control of Pneumatic Artificial Muscles Using a Fuzzy PD+I Controller

Original Scientific Paper

Vinh-Phuc Tran
Can Tho University,
Faculty of Automation Engineering, Automation Lab
3/2 Street, Can Tho, Vietnam
phuctv@vlute.edu.vn

Chi-Ngon Nguyen
Can Tho University,
Faculty of Automation Engineering
3/2 Street, Can Tho, Vietnam
ncngon@ctu.edu.vn

Nhut-Thanh Tran
Can Tho University,
Faculty of Automation Engineering
3/2 Street, Can Tho, Vietnam
nhutthanh@ctu.edu.vn

Chanh-Nghiem Nguyen*
Can Tho University,
Faculty of Automation Engineering, Automation Lab
3/2 Street, Can Tho, Vietnam
ncnghiem@ctu.edu.vn

*Corresponding author

Abstract *– This study evaluates the effectiveness of a fuzzy PD+I (FPD+I) controller for robust and adaptive position control of pneumatic artificial muscles (PAMs), addressing the challenges arising from system nonlinearity and hysteresis. Experiments were conducted under varying loads, setpoints, and actuated distances to assess the robustness and adaptability of the controller under diverse conditions. As part of the evaluation, the results were compared with those obtained using a conventional PID controller. The FPD+I controller consistently demonstrated superior transient response characteristics, improved trajectory-tracking accuracy, and greater adaptability to dynamic operational changes. Notable improvements include a 21% reduction in settling time and a 22% reduction in rise time under constant loads, as well as a 49% improvement in root mean square error and a 24% reduction in rise time during trajectory-tracking tasks. The controller also exhibited enhanced resilience to continuous load disturbances and maintained stable performance under varying signal amplitudes. These findings suggest that the FPD+I controller is a promising solution for precision control applications in robotics and industrial systems employing PAMs, particularly in dynamic and uncertain environments, where both robustness and adaptability are critical.*

Keywords: *Pneumatic artificial muscle (PAM), fuzzy PD+I control, adaptive control, robust control, position control*

Received: May 5, 2025; Received in revised form: July 7, 2025; Accepted: July 24, 2025

1. INTRODUCTION

A pneumatic artificial muscle (PAM) is a type of soft actuator that mimics the function of biological muscles using compressed air to generate force and motion. A PAM consists of a rubber tube encased in a braided mesh, which creates a contraction motion when pressurized [1]. When air is pumped in, the rubber tube expands radially and contracts longitudinally, generating pulling force and torque [2]. PAMs have the advantages of being lightweight, flexible, and capable of producing forces many times greater than their weight [3, 4]. These characteristics make PAMs ideal choices for applications in robotics [5], medical rehabilitation devices [6, 7], and industrial automation systems [8, 9]. However, controlling PAMs presents challenges because of their nonlinear characteristics, variability in pneumatic pressure parameters [10, 11], and dynamic hysteresis [12]–[14], which complicate the control process [15-17]. Additionally, air temperature and pressure also affect the PAM performance [18], [19]. Therefore, developing adaptive and efficient controllers to address these limitations is essential for fully exploiting the potential of PAMs in practical applications. This research area has attracted significant attention from both the scientific and engineering communities.

Over the past decade, various control approaches have been proposed to address these challenges. One major direction involves hysteresis compensation to overcome the system's nonlinearity and dynamic hysteresis. Many hysteresis compensation methods were proposed based on different variants of Prandtl-Ishlinskii (PI) models. Among them, based on the extended unparallel Prandtl-Ishlinskii, an integral inverse-proportional-integral-derivative controller can improve the control precision by 43.86% in comparison with a conventional proportional–integral–derivative (PID) controller without hysteresis compensation [15]. The feedforward and feedback combined control strategies demonstrated a maximum translational error of approximately 0.9 mm (i.e., 0.604% of the full stroke) [20] and a maximum tracking error of the rotation angle of the delta mechanism of ± 0.7° [16] in response to a low-frequency input sinusoidal signal of 0.1 Hz. However, these approaches require complex PAM modeling in real-world systems. Feasible employment of such controllers also requires them to withstand external disturbances and variations in operating conditions [21], which were not comprehensively reported in recent studies.

Although model-based identification methods have also been proposed and demonstrated promising results in accurately modeling the nonlinear dynamics of PAM actuators [22, 23], methods integrating hysteresis modeling and compensation have recently attracted research focus. For instance, Zhang et al. (2024) developed a dynamic model capturing coupled, stiffness- and rate-dependent hysteresis in soft PAM manipulators [24]. Their decoupled inverse compensation strategy improved positioning accuracy and highlighted the complexity of controlling variable-stiffness actuators. Another promising approach is model predictive control (MPC), which can anticipate system behavior and adjust control actions accordingly. Brown and Xie (2025) proposed a PSO-optimized MPC framework that outperformed traditional PID and iterative learning controllers in terms of accuracy and responsiveness in a rehabilitation setting [25]. Zhang et al. (2024) further demonstrated the potential of a disturbance preview-based predictive control strategy, which combined with hysteresis compensation and high-order differentiators, enabled robust trajectory tracking and model simplification for PAM-driven robots [26].

Despite their effectiveness, these methods often require complex system modeling, accurate hysteresis characterization, and high computational resources, making them less practical for real-time control in uncertain and dynamically changing environments. This limitation has led to increasing interest in classical or intelligent control schemes that do not compensate for hysteresis but ensure control effectiveness under certain conditions. Conventional PID controllers have proven to be effective in applications that do not require fast responses or industrial processes, where highly accurate positioning is not very demanding [27, 28]. Phuc et al. (2022) demonstrated an acceptable translational position control of a 25-kg payload with a settling time of only 1 s, insignificant overshoot, and a 0.35-mm steady-state error [27]. A rising time of 8.5 s and steady-state error of 5.129 mm were obtained by a PID controller when controlling the angle of an antagonistic dual-PAM system [28]. When higher positioning accuracy is prioritized, intelligent control systems are generally implemented to tackle PAM nonlinearity due to hysteresis. For example, high-order sliding mode control can be used to control a PAM-actuated robot arm that can follow an objective circular locus with a maximum error of approximately 11.3 mm [29]. To assist rehabilitation exercises, an adaptive sliding controller with a PID compensator can improve the tracking accuracy and reduce the steady-state tracking error of a robotic arm to below 5° [4]. A fuzzy sliding mode controller can be implemented with a steady-state error of 0.003°, satisfying the requirement of high accuracy for lower-limb systems [30]. Based on iterative real-time learning of Generative Adversarial Nets, a PID controller maintains effective tracking performance of antagonistic pneumatic artificial muscles under variations in their initial conditions, target angles, and external disturbances, demonstrating an advancement towards practical utilization of prostheses [31].

Despite advancements in PAM control strategies, several challenges remain in achieving robust and precise control under various operating conditions. A key area of focus is to improve the adaptability of control systems to handle a wider range of uncertainties and disturbances. For instance, the adaptive fixed-time fast terminal sliding mode control proposed by Khajehsaeid et al. (2025) demonstrated robustness against model uncertainties, assuming a 10% difference between actual and nominal link masses [32]. However, real-world applications may involve even greater variations in system parameters and external disturbances. Similarly, the adaptive control strategy presented by Sun et al. (2020) for PAM systems with parametric uncertainties and unidirectional input constraints exhibited resilience to more significant load variations from 0.633 to 1.633 kg and external disturbances applied at specific time intervals [17]. Although these results are promising, further research is required to expand the range of uncertainties and disturbances that can be effectively managed. In the context of lower-limb robotics, Tsai and Chiang (2020) demonstrated the effectiveness of a fuzzy sliding mode controller in achieving high accuracy, with steady-state errors of 0.003° without load and 0.00338° with a 2 kg load [30]. This level of precision is crucial for rehabilitation and assistive device applications. However, the performance of such controllers under more dynamic conditions, particularly when subjected to unexpected external forces, requires further investigation.

Another issue is that an effective control system must adapt to the continuous changes of the system dynamics. This capability enhances the operational performance and broadens the application range of PAM in di-

verse environments and tasks. Possible solutions include adaptive control or fuzzy-based strategies, as they have proven to be effective for external disturbances and varying system parameters [17], [30], [32]. Among fuzzy-based approaches, a combination of a fuzzy and PID controller is a feasible control scheme offering a compelling blend of simplicity, adaptability, good transient response, and accurate control. The fuzzy PD+I (FPD+I) controller, with its inherent adaptability and potential for high accuracy and quick response of position control, has emerged as a promising solution to meet the essential need for control strategies that can adapt to changing conditions in real time while maintaining adequate accuracy. Compared with a conventional PID controller with three branches of proportional, integral, and derivative components, the FPD+I controller comprises an adjustable fuzzy PD branch and a nonfuzzy integral component. The fuzzy PD branch is critical for the control system to dynamically adapt to the inherent nonlinearities and disturbances of the PAM and enable a fast response, whereas the nonfuzzy integral branch helps reduce the steady-state error [33]. This cumulative capacity is more pronounced than that of the PID controller. Thus, high control performance, flexible adaptability, and robustness can be achieved with FPD+I controllers in practical applications [34, 35]. Chan et al. (2003) further demonstrated that coupling an FPD+I controller with a learning control scheme enables accurate tracking control of PAMs [36], reinforcing its potential for robust and adaptive position control.

Despite these advancements, existing studies have not fully explored the potential of FPD+I controllers to address the combined challenges of nonlinearity, complex trajectory tracking, and continuous and complex disturbances in PAM systems. Therefore, this study specifically addresses the challenge of improving the accuracy and adaptability of PAM control under more complex operating conditions, particularly under different initial positions, tracking trajectories, and particularly continuously varying loads in a greater range, by deploying an FPD+I controller without any online learning scheme.

The main contributions of this study are summarized as follows:

- Development and real-time implementation of a fuzzy PD+I controller for PAM position control, eliminating the need for complex dynamic models or online adaptation mechanisms.
- Comprehensive experimental validation under a wide range of practical conditions, including fixed and continuously varying loads, multiple setpoints, and diverse trajectory profiles, to assess controller adaptability and robustness.
- Quantitative comparison with a conventional PID controller, demonstrating that the proposed FPD+I approach significantly improves tracking accuracy, reduces rise and settling times, and maintains performance under dynamic disturbances.
- A simple and practical controller design using a compact fuzzy rule base and no learning phase, enabling straightforward deployment in real-time embedded systems.

The remainder of this paper is organized as follows. Section 2 describes the experimental setup, system configuration, and the design of the proposed FPD+I control algorithm. Section 3 presents the experimental results along with a detailed performance analysis and a comparative evaluation against a conventional PID controller. Finally, Section 4 concludes the study by summarizing the key findings and outlining potential directions for future research.

2. MATERIALS AND METHODS

2.2. EXPERIMENTAL SETUPS

The experiment was conducted on a PAM with a diameter of 20 mm and an initial length of 200 mm (MAS-20-200N, FESTO). The PAM could shrink up to 20% of its original length, that is, a 40-mm distance, although a maximal 25% shrinkage at 6 bar has been reported for a new PAM [2]. The PAM displacement and pressure applied to the PAM were measured using an AccuracyTM KTC 100 rangefinder and Georgin SR13002A pressure sensor, respectively. Compressed air was supplied through a 5/3 proportional-directional control valve (MPYE-5-1/8-HF-101B; FESTO). The control and measurement algorithms were implemented using the MATLAB/Simulink software. All I/O data were transferred by using a Texas Instruments C2000 microcontroller (TMS320F28379D LaunchPAD). An overview of the proposed model is presented in Fig. 1.

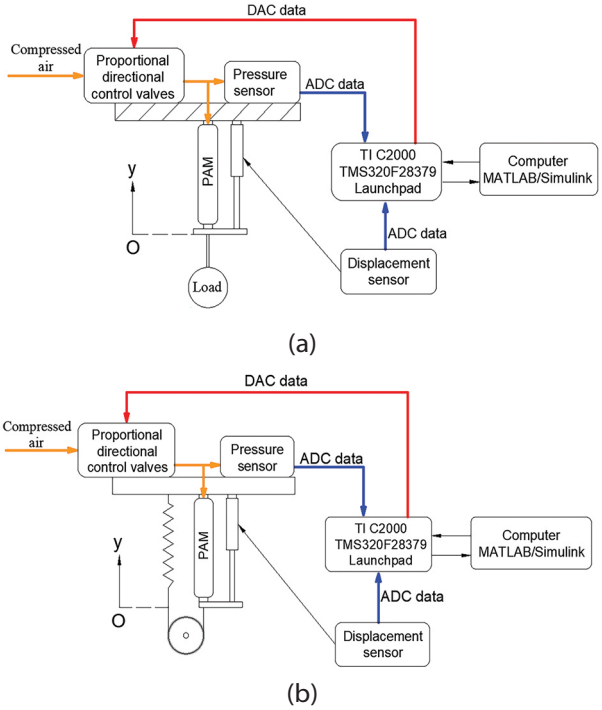

Fig. 1. Experimental setup with **(a)** constant load and **(b)** varying load

Six experiments were conducted in this study with two main goals: to investigate the effect of the load and the effect of different amplitudes and amplitude shifts of the input signal; hence, the setpoints and PAM's actuated distance on the position responses of the system. The experimental conditions and objectives are listed in Table 1. In Experiments 1.2 and 2.2, the robustness of the system was evaluated in response to direction changes in PAM actuation. This was done using 0.1 Hz rectangular pulse trains as reference inputs, formulated as

$$S_{A,c}(t) = A\,\mathrm{sgn}\left(\sin\left(\pi t / 5\right)\right) + c \tag{1}$$

where $sgn(.)$ is the sign function, A is the signal amplitude representing half the required actuated distance of the PAM, and c is the amplitude shift defining the initial position around which the bidirectional displacement of the PAM occurs. Both A and c were selected such that the reference input remained within the controllable range of the PAM.

To further explore the robustness of the system to continuously varying disturbances, a spring was added to the PAM's actuating head in Experiments 1.3 and 2.3, as shown in Fig. 1b. This spring was preloaded to create an initial elastic force simulating an equivalent static mass. As the PAM was actuated, the spring displacement increased, generating a continuous load disturbance that tested the robustness of the system under dynamic loading conditions.

Table 1. Conditions and goals of the position control experiments

Experiment No.	Main goal	Conditions		
		Description	Reference input (mm)	Mass (kg)
1.1	Investigate the effect of various disturbances on the load	Step input with various fixed loads	20	{15, 20, 25}
1.2		Rectangular pulse train with various fixed loads	$S_{5,10}(t)$=5 $sgn(sin(\pi t/5))$+10	{15, 20, 25}
1.3		Step input with disturbances to different simulated loads	20	Varying load from an initial equivalent load of {15, 20, 25} kg
2.1	To investigate the effect of different amplitudes and amplitude shifts of the input signal	Step input of different amplitudes	{10, 20, 30}	20
2.2		Rectangular pulse trains of different amplitudes and amplitude shifts	$S_{A,c}(t)$=A $sgn(sin(\pi t/5))$+c where c∈{15,20,25}, A∈{3,5}	20
2.3		Step input of different amplitudes with disturbances to a simulated load	$S_{A,c}(t)$=A $sgn(sin(\pi t/5))$+c where c∈{15,20,25}, A∈{3,5}	Varying load from an initial equivalent load of 20 kg

2.2. CONTROL ALGORITHMS

As shown in Fig. 2, the control system includes two nested control loops. The inner control loop employs a PI controller to regulate the air pressure, ensuring stability for the outer loop to govern the PAM position. The PI controller receives the control signal u and the measured air pressure P from a pressure sensor to generate a pressure control signal, which is then applied to the proportional electro-pneumatic valve, maintaining consistent and stable pressure regulation.

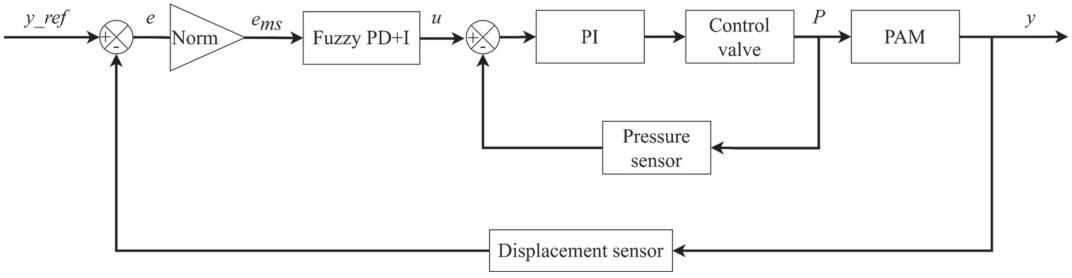

Fig. 3. Structure of the fuzzy PD+I control system

In the outer loop, an FPD+I controller manages the position control. It receives the position error signal e, calculated as the difference between the reference input y_ref and the measured PAM displacement y. The error is normalized by a Norm block to scale its magnitude appropriately. The FPD+I controller then processes the normalized error ems to generate the control signal u for the inner PI control loop. The normalized error is measured as the percent error with respect to the maximal shrinkage from its idle position, calculated as:

$$e_{ms}(k) = \frac{e(k)}{40} \times 100\% \tag{2}$$

The combined action of the outer FPD+I controller and the inner PI controller enables precise control of the PAM position while compensating for pressure fluctuations and external disturbances. The displacement sensor continuously measures the actual position y, thereby closing the outer feedback loop. A summary of the signals shown in Fig. 2 is presented in Table 2.

Table 2. Main signals in the control system

Parameter	Description	Unit
y_{ref}	Reference displacement input	mm
y	Measured displacement output	mm
e	Position error ($e = y_{ref} - y$)	mm
e_{ms}	Normalized error	%
u	Control signal applied to the inner control loop	%
P	Measured air pressure inside PAM	bar

2.2.1. PI controller

The pressure inside the PAM depends on the nonlinearity of the airflow through the proportional directional control valve, volume variation, air temperature, and air leakage through the valve. Therefore, to ensure a stable air pressure, a PI controller was implemented. The controller gains were empirically determined and kept constant in all experiments at $K_P = 2$ and $K_I = 4.6$.

2.2.2. PID controller

The PID controller computes the control signal $u_{PID}(k)$ at each discrete time step k based on the time-domain error between the desired position and actual measured position of the PAM, as follows:

$$u_{PID}(k) = K_P \cdot e_{ms}(k) + K_I \cdot \sum_{i=0}^{k} e_{ms}(k) \cdot T_s + K_D \cdot \frac{e_{ms}(k) - e_{ms}(k-1)}{T_s} \quad (3)$$

where K_P, K_I, and K_D are the proportional, integral, and derivative gains of the PID controller, respectively, and $e_{ms}(k)$ is the percent error at time step k.

The gains of the PID controller were empirically determined to be $K_P = 0.2$, $K_I = 1.0$, and $K_D = 0.01$. The sampling period Ts was 0.01 s.

2.2.3. Fuzzy PD+I controller

An FPD+I controller, whose structure is shown in Fig. 3, was built to control the position of the PAM. A Mamdani fuzzy inference system (FIS) was implemented using the Fuzzy Logic Toolbox, MATLAB.

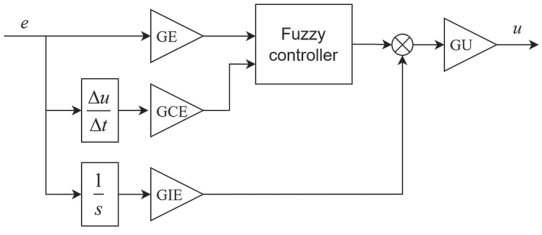

Fig. 3. The FPD+I structure

The output from the fuzzy PD branch of the FPD+I controller at time k is calculated as:

$$u_{FPD}(k) = F\left(e_{ms}(k), de_{ms}(k)\right) \quad (4)$$

where $F(.)$ denotes the mapping realized by the fuzzy rule base with the Gaussian membership functions.

The output from the integral branch of the FPD+I controller component is defined as

$$u_I(k) = GIE \sum_{i=0}^{k} e(i) \cdot T_s \quad (5)$$

The control output of the FPD+I controller is a combination of the outputs from the fuzzy PD and integral branches, calculated as follows:

$$u(k) = GU * \left[u_{FPD}(k) + u_I(k)\right] \quad (6)$$

where GU is the overall gain-scaling factor.

Seven Gaussian membership functions were defined based on the percent error e_{ms} and the derivative of the percent error. Fuzzy control rules were established, as listed in Table 3. The response surface based on these control rules is shown in Fig. 4. The crisp output of the FPD+I controller obtained from the fuzzy variables agrees with that of a previous report [37].

The range of the control output u was [0, 100%], corresponding to the airflow capacity of the pneumatic valve. The proportional gains GE, GCE, GIE, and GU (Fig. 2) were determined to satisfy the operating limit of the controller's input so that [38]

$$GE * GU = K_P \quad (7)$$

$$GCE/GE = T_D \quad (8)$$

$$GIE/GE = 1/T_I \quad (9)$$

where $K_P = 0.2$, $T_I = 0.2$, and $T_D = 0.05$, which were empirically selected and remained unchanged during the tests.

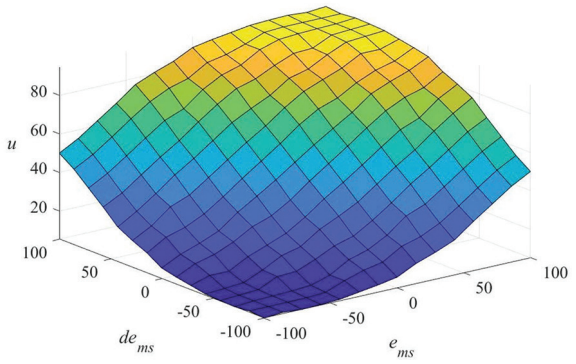

Fig. 4. The response surface

Table 3. Fuzzy rules for controlling PAM position

e_{ms} ∈ [-100, 100%]	de_{ms} ∈ [-100, 100%]						
	NL	NM	NS	Z	PS	PM	PL
VVS	VVS	VVS	VVS	VVS	VS	S	M
VS	VVS	VVS	VVS	VS	S	M	L
S	VVS	VVS	VS	S	M	L	VL
M	VVS	VS	S	M	L	VL	VVL
L	VS	S	M	L	VL	VVL	VVL
VL	S	M	L	VL	VVL	VVL	VVL
VVL	M	L	VL	VVL	VVL	VVL	VVL

VVS: very very small; VS: very small; S: small; M: medium; L: large; VB: very large; VVB: very very large; NL: negatively large; NM: negatively medium; NS: negatively small; Z: zero; PS: positively small; PM: positively medium; PL: positively large.

A conventional PID controller was designed through trial and error for comparison with the FPD+I controller. The initial proportional, integral, and derivative gains of the PID controller were empirically determined and adjusted to balance the rise time, settling time, and overshoot, thereby ensuring its effectiveness under typical operating conditions without excessive oscillations or delays.

2.3. EVALUATION OF THE MODEL PERFORMANCE

Root mean squared error (RMSE) is selected to quantitatively evaluate the response of the position controller, calculated as

$$RMSE = \sqrt{\sum_{i=1}^{N} \frac{\left(y_i - \hat{y}_i\right)^2}{N}} \tag{10}$$

where $\hat{y}_i$ is the response of the corresponding set-point value $\hat{y}_i$ in the dataset of N samples. In this study, the PAM displacement and RMSE were computed in millimeters.

The system performance was also evaluated based on the transient response characteristics, including the percent overshoot (POT), rise time, and settling time, under various experimental conditions and setups. Because of the low response characteristic of PAM, the rise time was calculated as the time required for the response to increase from 0% to 90% of its reference value (rather than its final value). For better reference, the percent of improvement (PoI) was calculated to show the relative performance improvement in a certain performance metric, including RMSE, POT, rise time, and settling time, as

$$PoI = \frac{m_{PID} - m_{FPD+I}}{m_{PID}} \times 100\% \tag{11}$$

where m_{FPD+I} and m_{PID} are the values of a performance metric (i.e., RMSE, POT, rise time, or settling time) obtained using the FPD+I and PID controllers, respectively. A positive PoI indicates an enhancement in control performance compared to the baseline PID controller, whereas a negative PoI implies a deterioration of the desired response.

To evaluate the effect of load disturbances, the percent of degradation (PoD) was formulated to show the performance degradation in a performance metric as follows:

$$PoD = \frac{\left|\bar{m}_{disfree} - \bar{m}_{dis}\right|}{\bar{m}_{disfree}} \times 100\% \tag{12}$$

where $\bar{m}_{dis}$ and $\bar{m}_{disfree}$ are the mean values of a performance metric (i.e., POT, rise time, or settling time) obtained with and without the load disturbances, respectively. The PoD reflects the extent to which external disturbances degrade the system with respect to a performance metric. Therefore, PoI and PoD provide a systematic and quantitative basis for assessing both the effectiveness of the proposed control strategy and its robustness under varying operating conditions.

3. RESULTS AND DISCUSSION

3.1. EFFECT OF LOAD ON THE POSITION RESPONSE

3.1.1. Experiment 1.1: Step response analysis under different loads

In Experiment 1.1, a set-point position of $r = 20$ mm was applied to the system under loads of 15 kg, 20 kg, and 25 kg. The corresponding step responses are shown in Fig. 5. The performance of the FPD+I and PID controllers are listed in Table 4. Compared with the PID controller, the FPD+I controller had a lower POT, shorter rise time, and shorter settling time of at least 14%, 22%, and 21%, respectively, than the PID controller. These results demonstrate its superior performance compared with the PID controller in transient responses under different loads.

3.1.2. Experiment 1.2: Trajectory tracking with a rectangular pulse train under varying loads

In this experiment, a 0.1-Hz rectangular pulse train $S5{,}10\,(t)=5\,sgn(sin(\pi t/5))+10$ was applied as the reference input to the system under different loads of 10, 20, and 25 kg. In addition to evaluating the load effects on the position control performance, this experiment was conducted to partly evaluate the robustness of the control system in response to a tracking trajectory of higher complexity.

As shown in Fig. 6, the FPD+I controller exhibits quicker responses than the conventional PID controller. Compared with the PID controller, the FPD+I controller reduced the RMSE and rise time by 49% and 24%, respectively (Table 5), demonstrating that the FPD+I controller was more accurate and robust for complex trajectory-tracking applications under significant load variations of 15–25 kg.

It should be noted that an insignificant overshoot was observed with the FPD+I controller, whereas the system exhibited an underdamped response, that is, the PAM could not reach the desired setpoint when using the PID controller.

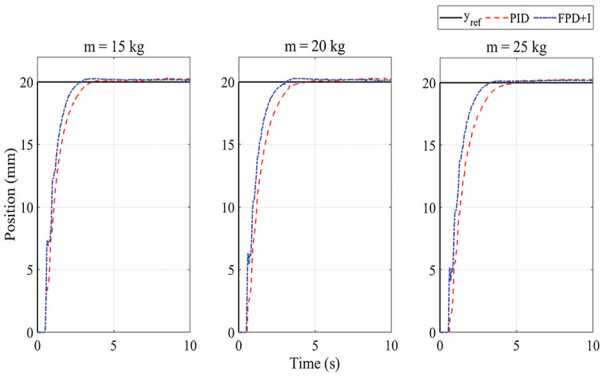

Fig. 5. Step responses under different loads (Experiment 1.1)

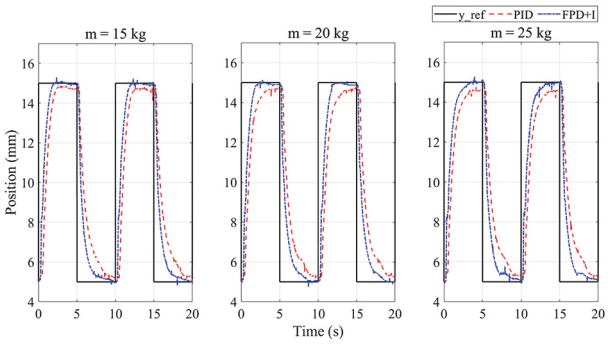

Fig. 6. Position responses of the PAM with different loads to a 0.1 Hz rectangular pulse train (Experiment 1.2)

3.1.3. Experiment 1.3: Step response analysis under varying simulated loads with continuous load disturbances

Experiment 1.3 was conducted in alignment with Experiment 1.1. However, the corresponding loads were simulated using the equivalent elastic force of a string with a proper displacement. Based on the setup shown in Fig. 1b, a continuous load disturbance can be applied to the system to evaluate the robustness of the FPD+I controller. As the PAM reached setpoint r = 20 mm, the elastic force increased, leading to equivalent load increases of 130%, 131%, and 155% from the initial simulated loads of 15, 20, and 25 kg, respectively. Fig. 7 shows the step responses of the PAM system under different simulated loads with continuous disturbances. The detailed system performance is listed in Table 6. Because of these significant and continuous load disturbances, minor POTs were observed, and the settling and rise times were greater than those of the corresponding disturbance-free cases in Experiment 1.1 (Table 4).

Based on the average performance metrics summarized in Table 7, the FPD+I controller consistently outperformed the PID controller under continuous load disturbances. Although both controllers exhibited performance degradation in the presence of dynamic loads, the FPD+I controller demonstrated greater robustness, as reflected by the smaller increases in rise and settling times. Specifically, the FPD+I controller experienced increases of only 0.5 s in rise time and 0.8 s in settling time, compared to larger increases of 0.7 s and 1.0 s, respectively, for the PID controller. Furthermore, the slightly lower percent of degradation (PoD) values observed for the FPD+I controller (Table 8) further confirm its superior resilience to continuous external disturbances.

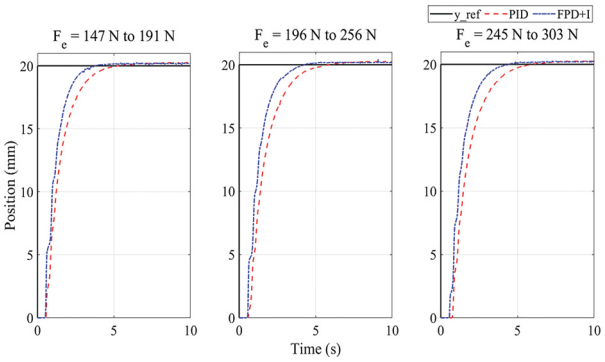

Fig. 7. Position response of PAM with varying elastic forces simulated by springs (Experiment 1.3)

Table 4. Performance of FPD+I and PID controllers under different loads (Experiment 1.1)

	POT			Rise time			Settling time		
Mass (kg)	FPD+I (%)	PID (%)	*Pol* (%)	FPD+I (s)	PID (s)	*Pol* (%)	FPD+I (s)	PID (s)	*Pol* (%)
15	1.5	1.9	21	2.1	2.7	22	2.4	3.1	23
20	1.4	2.2	36	2.3	3.0	23	2.7	3.4	21
25	1.8	2.1	14	2.5	3.2	22	2.8	3.9	28

Table 5. Performance of FPD+I and PID controllers in response to a 0.1 Hz rectangular pulse train under different loads (Experiment 1.2)

	RMSE			Rise time		
Mass (kg)	FPD+I (mm)	PID (mm)	*Pol* (%)	FPD+I (s)	PID (s)	*Pol* (%)
15	1.7	3.7	54	1.6	2.1	24
20	1.9	3.9	51	1.6	3.1	48
25	2.0	3.9	49	2.2	3.3	33

Table 6. Performance of the FPD+I and PID controllers under different simulated loads with continuous load disturbances (Experiment 1.3)

	POT			Rise time			Settling time		
Equivalent mass (kg)	FPD+I (%)	PID (%)	*Pol* (%)	FPD+I (s)	PID (s)	*Pol* (%)	FPD+I (s)	PID (s)	*Pol* (%)
15	1.4	1.7	18	2.5	3.4	26	3.0	4.0	25
20	1.9	2.1	10	2.9	3.8	24	3.6	4.6	22
25	1.3	1.7	24	3.0	4.0	25	3.6	4.8	25

Table 7. Average performance of FPD+I and PID controllers with and without continuous load disturbances

	FPD+I controller		PID controller	
Metrics	**Exp. 1.1**	**Exp. 1.3**	**Exp. 1.1**	**Exp. 1.3**
RMSE	3.6 mm	3.9 mm	4.0 mm	4.3 mm
POT	1.6%	1.5%	2.1%	1.8%
Settling time	2.6 s	3.4 s	3.5 s	4.5 s
Rise time	2.3 s	2.8 s	3.0 s	3.7 s

Table 8. Performance degradation of FPD+I and PID controllers due to load disturbances

Metrics	FPD+I	PID
POT	-2,1%	-11,3%
Settling time	29,1%	28,8%
Rise time	21,7%	25,8%

PoD was calculated without rounding up the mean values of a certain metrics

In addition to robustness, the FPD+I controller exhibited better adaptability to dynamic load variations, as indicated by its smaller performance degradation relative to the conventional PID controller, without the need for controller retuning. Quantitatively, the FPD+I controller reduced the percent degradation in the rise and settling times by approximately 29% and 20%, respectively, compared to the PID controller.

3.2. EFFECT OF THE AMPLITUDE OF THE INPUT SIGNAL

3.2.1. Experiment 2.1: Step responses analysis with varying setpoints

The objective of this experiment was to evaluate the ability of the controller to maintain performance across different setpoints compared with a conventional PID controller. A fixed load of 20 kg was applied, and step responses were obtained at setpoint positions of 10, 20, and 30 mm. It should be noted that the step response for r = 20 mm was obtained in Experiment 1.1.

As shown in Table 9 and Fig. 8, the FPD+I controller generally exhibited faster transient responses than the PID controller, particularly at larger setpoint changes. For the short actuated distance of r = 10 mm, the FPD+I controller did not outperform the PID controller in terms of the rise time. The rise time of the FPD+I controller was slightly longer by approximately 2.4%. Although it achieved a significantly faster settling time, reducing it by approximately 2.4 seconds compared to the PID controller, the overshoot resulted in oscillations, causing the final settling time to increase substantially to 5.9 seconds. This value was at least 200% longer than those observed at larger setpoints (r = 20 mm and 30 mm, where settling times were 2.5 s and 2.8 s, respectively).

At longer actuated distances (r = 20 and 30 mm), the FPD+I controller demonstrated substantial improvements in rise time, achieving enhancements of more than 31% compared to the PID controller. However, no significant improvement was observed in the POT compared to the PID controller.

In all cases, the FPD+I controller consistently outperformed the PID controller in terms of settling time. These results highlight the superior transient performance of the FPD+I controller, particularly for larger signal amplitudes. Overall, the findings underscore the controller's superior adaptability to varying setpoint commands and its robustness in maintaining the control performance under different operating demands.

It should also be noted that actuating the PAM initially from the zero position introduced a baseline delay because the muscle needed to inflate before contraction could generate an actuated force. This inflation delay averaged approximately 0.49 seconds and was included in the calculated rise and settling times.

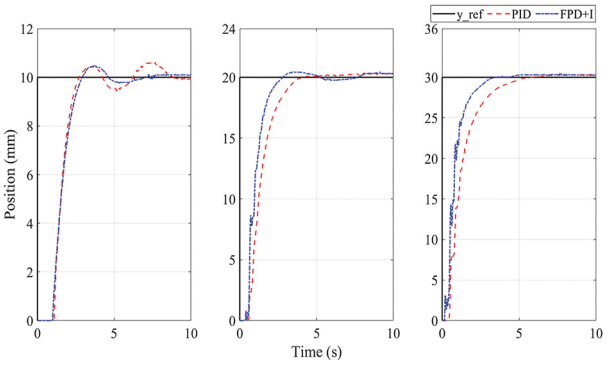

Fig. 8. Position control performance across different setpoints under a 20 kg load (Experiment 2.1)

Table 9. Characteristics of transient responses of FPD+I and PID controllers across varying setpoints (Experiment 2.1)

	POT			Rise time			Settling time		
Position setpoint (mm)	**FPD+I (%)**	**PID (%)**	***PoI* (%)**	**FPD+I (s)**	**PID (s)**	***PoI* (%)**	**FPD+I (s)**	**PID (s)**	***PoI* (%)**
10	4.8	6.2	23	2.61	2.55	-2.4	5.9	8.3	29
20	2.3	2.2	-5	2.12	3.09	31.4	2.5	3.6	31
30	1.7	1.6	-6	2.27	3.5	35.1	2.8	4.5	38

3.2.2. Experiment 2.2: Trajectory tracking with rectangular pulse trains of different amplitudes

This experiment aimed to assess the control system's robustness and adaptability in tracking more complex trajectories. A 0.1-Hz rectangular pulse train was applied as the reference input, with varying amplitudes (A = 3 mm and 5 mm) and amplitude shifts (c = 10, 15, and 25 mm) to evaluate the system performance under different actuated distances of the PAM. The setup was similar to that of Experiment 1.2, but with additional variations to increase the tracking difficulty.

As shown in Fig. 9 and Tables 10–11, the FPD+I controller consistently achieved faster responses than the PID controller, which is consistent with the observations from Experiment 1.2. Specifically, the FPD+I controller achieved notable reductions in rise time, with average improvements of approximately 41% and 32% for amplitudes of 3 and 5 mm, respectively (Table 10).

In terms of positional accuracy, the FPD+I controller outperformed the PID controller, as indicated by the lower RMSE values. The average improvements in the RMSE were approximately 21% and 19% for amplitudes of 3 mm and 5 mm, respectively (Table 11).

It is worth noting that the FPD+I controller exhibited minimal overshoot, indicating good transient behavior, even under complex reference signals. In contrast, the PID controller produced an underdamped response, where the PAM failed to effectively reach the desired setpoints. These results demonstrate the superior robustness and adaptability of the FPD+I controller for managing varying trajectory profiles and actuation distances.

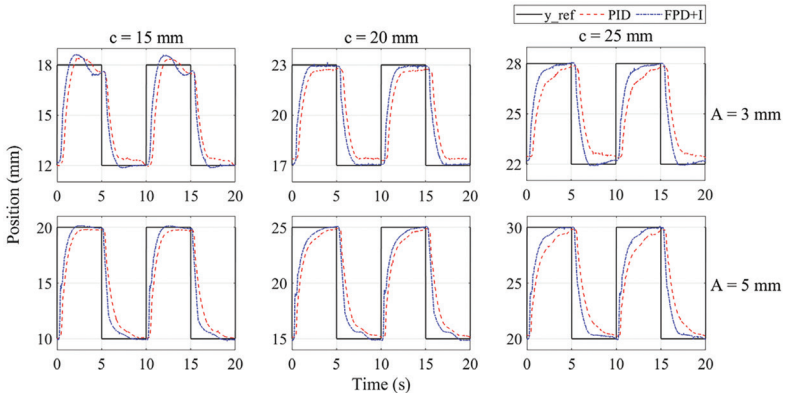

Fig. 9. PAM position control performance under varying amplitudes (A = 3 mm and 5 mm) and amplitude shifts (c = 10–25 mm) using FPD+I and PID controllers (Experiment 2.2)

Table 10. Rise time comparison for the FPD+I and PID controllers with varying amplitudes and amplitude shifts (Experiment 2.2)

Amplitude shift *c* (mm)	Amplitude A = 3 mm			Amplitude A = 5 mm		
	FPD+I	PID	*PoI* (%)	FPD+I	PID	*PoI* (%)
10	1.2	1.7	29	1.5	2.2	32
15	1.7	3.7	54	2.6	3.6	28
25	2.5	4.2	40	2.9	4.6	37
Average	1.8	3.2	41	2.3	3.5	32

Table 11. RMSE comparison for the FPD+I and PID controllers with varying amplitudes and amplitude shifts (Experiment 2.2)

Amplitude shift *c* (mm)	Amplitude A = 3 mm			Amplitude A = 5 mm		
	FPD+I	PID	*PoI* (%)	FPD+I	PID	*PoI* (%)
10	2.0	2.4	17	3.0	3.7	19
15	2.0	2.6	23	3.3	4.0	18
25	2.1	2.7	22	3.3	4.2	21
Average	2.0	2.6	21	3.2	4.0	19

3.2.3. Experiment 2.3: Evaluation of system robustness in trajectory tracking under continuous load disturbances

Similar to Experiment 1.3, this experiment used a spring with an initial deformation to simulate a 20 kg load, introducing a continuous load disturbance due to the changing opposing elastic force during PAM contraction. However, rectangular pulse trains similar to those used in Experiment 2.2 were applied as reference inputs to evaluate the robustness of the system in complex trajectory tracking with varying actuated distances of the PAM under continuous disturbances.

The results in Tables 12 and 13 demonstrate that the FPD+I controller outperformed the conventional PID controller in terms of both the tracking accuracy and response speed under continuous load disturbances. Specifically, the FPD+I controller achieved lower RMSE values across all tested conditions, with average improvements of 18% and 21% for amplitudes A of 3 mm and 5 mm, respectively (Table 12). Similarly, the rise time was significantly reduced, with the FPD+I controller achieving improvements of 34% and 35% compared to the PID controller for amplitudes of 3 mm and 5 mm, respectively (Table 13).

In addition to the improved accuracy and faster responses, it is noteworthy that the FPD+I controller exhibited only an insignificant overshoot, indicating good transient performance (Fig. 10). Conversely, the PID controller resulted in an underdamped response, where the PAM struggled to reach the desired setpoints under the influence of varying load disturbances, particularly for longer actuated distances. These results further confirm the robustness and effectiveness of the FPD+I controller in complex trajectory-tracking scenarios.

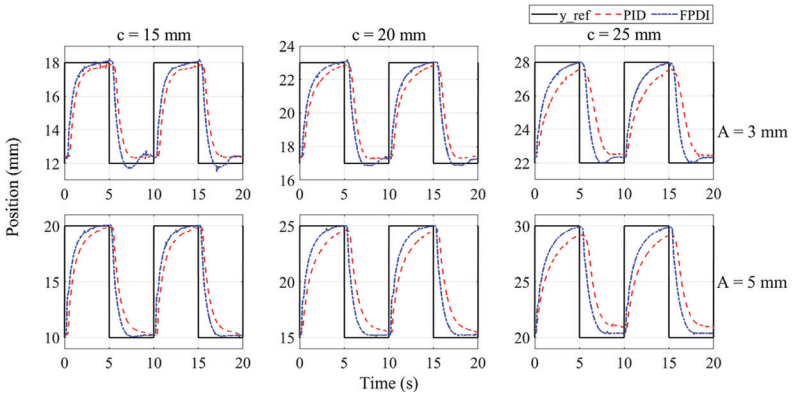

Fig. 10. PAM position response under elastic force with 0.1 Hz square wave input (Experiment 2.3)

Table 12. RMSE comparison for FPD+I and PID controllers with varying amplitudes and amplitude shifts (Experiment 2.3)

Amplitude shift *c* (mm)	Amplitude A = 3 mm			Amplitude A = 5 mm		
	FPD+I	PID	*PoI* (%)	FPD+I	PID	*PoI* (%)
10	2.1	2.5	16	3.2	3.9	18
15	2.2	2.6	15	3.3	4.3	23
25	2.2	2.8	21	3.5	4.5	22
Average	2.2	2.6	18	3.3	4.2	21

Table 13. Rise time comparison for the FPD+I and PID controllers with varying amplitudes and amplitude shifts (Experiment 2.3)

Amplitude shift *c* (mm)	Amplitude A = 3 mm			Amplitude A = 5 mm		
	FPD+I	PID	*PoI* (%)	FPD+I	PID	*PoI* (%)
10	2.4	3.9	38	2.5	3.7	32
15	2.9	4.4	34	3	4.8	38
25	3.5	4.9	29	3.5	5.4	35
Average	2.9	4.4	34	3.0	4.6	35

3.3. ADAPTABILITY ANALYSIS

To further evaluate the performance of the FPD+I controller beyond individual experiments, its adaptability under dynamic and uncertain operating conditions was analyzed. In this context, adaptability refers to the controller's ability to maintain high tracking accuracy and stable transient responses despite variations in load, setpoint amplitudes, and external disturbances. As summarized in Table 14 and illustrated in Fig. 11, the FPD+I controller consistently maintained a lower RMSE, faster rise times, and shorter settling times across a wide range of operating conditions including fixed and varying loads, different setpoints (10–30 mm), and continuous load disturbances (up to 155% equivalent mass increase). Compared to the conventional PID controller, the FPD+I controller exhibited significantly smaller performance variations, demonstrating superior robustness and adaptability.

Fig. 11 shows that while the PID controller's tracking accuracy and transient behavior degraded noticeably under changing conditions, the FPD+I controller maintained a stable performance with minimal degradation. These findings confirm that the FPD+I controller can dynamically adjust to real-time variations in system behavior without requiring model-based compensation or parameter

Table 14. Performance consistency of FPD+I controller across different operating conditions

Condition type	Variation range	Performance (RMSE, rise time, settling time)	Evaluation remarks
Load variations	15–25 kg (fixed and varying)	Consistent; low RMSE; rise/settling times slightly affected	Robust to large static and dynamic load changes
Setpoint variations	10–30 mm	Minimal impact on transient response; minor overshoot for the smaller setpoints	Good adaptability to different target positions; significant increase in settling time for small setpoint (r = 10 mm)
Signal amplitude and amplitude shift	Amplitude: 3–5 mm; Amplitude shift: 15–25 mm	Maintained fast response and low error	Well adapted to varying amplitude shifts
Continuous load disturbance	130%–155% equivalent mass increase	Performance degradation <30%	High resilience under dynamic external forces

retuning. Overall, the results validated the effectiveness of the FPD+I controller in providing both robust and adaptive position control for pneumatic artificial muscles operating in dynamic and uncertain environments.

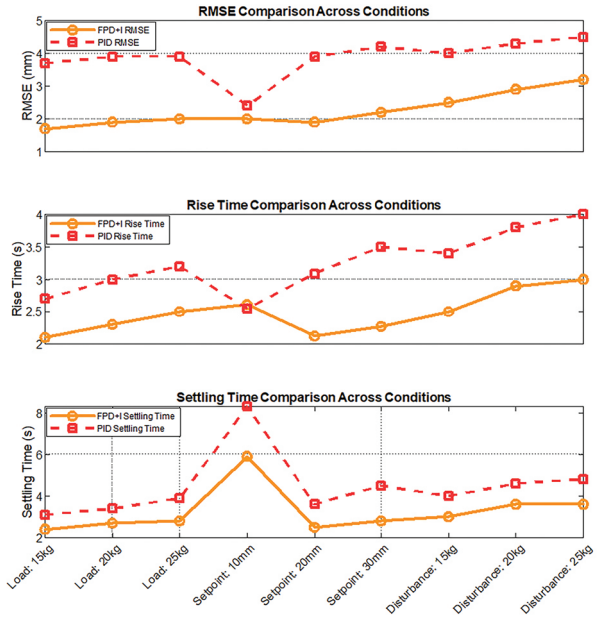

Fig. 11. Performance comparison of FPD+I and PID controllers across varying operating conditions in terms of RMSE, rise time, and settling time

4. CONCLUSIONS

This study investigated the robust position control of pneumatic artificial muscles (PAMs) using a fuzzy PD+I (FPD+I) controller to address the challenges arising from system nonlinearities, hysteresis, and external disturbances. The proposed controller was evaluated through a series of experiments involving various loads, setpoints, and actuated distances. The key results demonstrate that the FPD+I controller significantly outperformed a conventional PID controller, achieving superior transient response characteristics, including reductions of at least 21% in settling time and 22% in rise time and improvements in trajectory tracking accuracy (up to 49% reduction in RMSE). The FPD+I controller consistently maintained strong performance under diverse operating conditions, including continuous and dynamic load disturbances, thereby validating its robustness against uncertainties and external variations. Simultaneously, its ability to sustain high tracking accuracy and fast response across different setpoints, actuated distances, and complex trajectories confirmed its high adaptability without the need for model-based hysteresis compensation or retuning.

To contextualize these results, relevant comparisons with findings from previous studies are discussed. For instance, Phuc et al. (2023) reported steady-state errors of approximately 0.35 mm and settling times around 1 s using PID control under fixed load conditions [27]. In comparison, the present study demonstrated that similar or better levels of accuracy and responsiveness can be achieved without the need for retuning, even under dynamic and varying loads. Other approaches, such as the sliding mode controller used by Lin et al. (2021), showed maximum position errors of about 11.3 mm, whereas the proposed FPD+I controller achieved average RMSE values as low as 3.9 mm [29]. Moreover, while adaptive and fuzzy sliding mode controllers [4, 17, 30] have achieved high tracking accuracy, they often involve complex system modeling and extensive parameter tuning. The FPD+I controller, by contrast, provided competitive performance with a simpler design and implementation. These qualitative comparisons highlight the practical advantages of the proposed method in achieving robust and adaptive position control of PAMs across a wide range of operating conditions.

5. REFERENCES:

[1] M. Chavoshian, M. Taghizadeh, "Recurrent neuro-fuzzy model of pneumatic artificial muscle position", Journal of Mechanical Science and Technology, Vol. 34, No. 1, 2020, pp. 499-508.

[2] A. Festo, "Fluidic Muscle DMSP", 2007.

[3] D. H. Plettenburg, "Pneumatic actuators: a comparison of energy-to-mass ratio's", Proceedings of the 9th International Conference on Rehabilitation Robotics, Chicago, IL, USA, 28 June - 1 July 2005, pp. 545-549.

[4] H. T. Nguyen, V. C. Trinh, T. D. Le, "An Adaptive Fast Terminal Sliding Mode Controller of Exercise-Assisted Robotic Arm for Elbow Joint Rehabilitation Featuring Pneumatic Artificial Muscle Actuator", Actuators, Vol. 9, No. 4, 2020, p. 118.

[5] R. M. Robinson, C. S. Kothera, N. M. Wereley, "Variable Recruitment Testing of Pneumatic Artificial Muscles for Robotic Manipulators", IEEE/ASME Transactions on Mechatronics, Vol. 20, No. 4, 2015, pp. 1642-1652.

[6] A. Merola, D. Colacino, C. Cosentino, F. Amato, "Model-based tracking control design, implementation of embedded digital controller and testing of a biomechatronic device for robotic rehabilitation", Mechatronics, Vol. 52, 2018, pp. 70-77.

[7] S. Hussain, P. K. Jamwal, M. H. Ghayesh, S. Q. Xie, "Assist-as-needed control of an intrinsically compliant robotic gait training orthosis", IEEE Transactions on Industrial Electronics, Vol. 64, No. 2, 2017, pp. 1675-1685.

[8] G. Andrikopoulos, G. Nikolakopoulos, S. Manesis, "A Survey on applications of Pneumatic Artificial Muscles", Proceedings of the 19th Mediterranean Conference on Control & Automation, Corfu, Greece, 20-23 June 2011, pp. 1439-1446.

[9] T.-C. Tsai, M.-H. Chiang, "A Lower Limb Rehabilitation Assistance Training Robot System Driven by an Innovative Pneumatic Artificial Muscle System", Soft Robotics, Vol. 10, No. 1, 2023, pp. 1-16.

[10] S. Jamian et al. "Review on controller design in pneumatic actuator drive system", Telkomnika (Telecommunication, Computing, Electrical & Electronics, and Instrumentation & Control), Vol. 18, No. 1, 2020, pp. 332-342.

[11] B. Tondu, S. Ippolito, J. Guiochet, A. Daidie, "A Seven-degrees-of-freedom robot-arm driven by pneumatic artificial muscles for humanoid robots", The International Journal of Robotics Research, Vol. 24, No. 4, 2005, pp. 257-274.

[12] M. Al Saaideh, M. Al Janaideh, "On Prandtl-Ishlinskii Hysteresis Modeling of a Loaded Pneumatic Artificial Muscle", ASME letters in dynamic systems and control, Vol. 2, No. 3, 2022, pp. 1-12.

[13] S. Shakiba, M. Ourak, E. Vander Poorten, M. Ayati, A. Yousefi-Koma, "Modeling and compensation of asymmetric rate-dependent hysteresis of a miniature pneumatic artificial muscle-based catheter", Mechanical Systems and Signal Processing, Vol. 154, 2021, p. 107532.

[14] S. L. Xie, H. T. Liu, Y. Wang, "A method for the length-pressure hysteresis modeling of pneumatic artificial muscles", Science China Technological Sciences, Vol. 63, No. 5, 2020, pp. 829-837.

[15] L. Hao, H. Yang, Z. Sun, C. Xiang, B. Xue, "Modeling and compensation control of asymmetric hysteresis in a pneumatic artificial muscle", Journal of Intelligent Material Systems and Structures, Vol. 28, No. 19, 2017, pp. 2769-2780.

[16] P. Geng, Y. Qin, L. Zhong, F. Qu, D. Bie, J. Han, "Direct Inverse Hysteresis Compensation of a Pneumatic Artificial Muscles Actuated Delta Mechanism", Proceedings of the 10th Institute of Electrical and Electronics Engineers International Conference on Cyber Technology in Automation, Control, and Intelligent Systems, Xi'an, China, 10-13 October 2020, pp. 18-23.

[17] N. Sun, D. Liang, Y. Wu, Y. Chen, Y. Qin, Y. Fang, "Adaptive Control for Pneumatic Artificial Muscle Systems With Parametric Uncertainties and Unidirectional Input Constraints", IEEE Transactions on Industrial Informatics, Vol. 16, No. 2, 2020, pp. 969-979.

[18] P. A. Laski et al. "Study of the effect of temperature on the positioning accuracy of the pneumatic muscles", EPJ Web of Conferences, Vol. 143, 2017, p. 02065.

[19] T. Tagami, T. Miyazaki, T. Kawase, T. Kanno, K. Kawashima, "Pressure Control of a Pneumatic Artificial Muscle Including Pneumatic Circuit Model", IEEE Access, Vol. 8, 2020, pp. 60526-60538.

[20] Z. Song, L. Zhong, N. Sun, Y. Qin, "Hysteresis Compensation and Tracking Control of Pneumatic Artificial Muscle", Proceedings of the IEEE 9th Annual International Conference on CYBER Technology in Automation, Control, and Intelligent Systems, Suzhou, China, 29 July - 2 August 2019, pp. 1412-1417.

[21] Y. Qin, H. Zhang, X. Wang, J. Han, "Active Model-Based Hysteresis Compensation and Tracking Control of Pneumatic Artificial Muscle", Sensors, Vol. 22, No. 1, 2022, p. 364.

[22] C. Van Kien, N. N. Son, and H. P. H. Anh, "Identification of 2-DOF pneumatic artificial muscle system with multilayer fuzzy logic and differential evolution algorithm", Proceedings of the 12th IEEE Conference on Industrial Electronics and Applications, Siem Reap, Cambodia, 18-20 June 2017, pp. 1264-1269.

[23] N. N. Son, C. Van Kien, H. P. H. Anh, "A novel adaptive feed-forward-PID controller of a SCARA parallel robot using pneumatic artificial muscle actuator based on neural network and modified differential evolution algorithm", Robotics and Autonomous Systems, Vol. 96, 2017, pp. 65-80.

[24] Y. Zhang, Q. Cheng, W. Chen, J. Xiao, L. Hao, Z. Li, "Dynamic modelling and inverse compensation for coupled hysteresis in pneumatic artificial muscle-actuated soft manipulator with variable stiffness", ISA Transactions, Vol. 145, 2024, pp. 468-478.

[25] D. F. Brown, S. Q. Xie, "Model Predictive Control with Optimal Modelling for Pneumatic Artificial

Muscle in Rehabilitation Robotics: Confirmation of Validity Though Preliminary Testing", Biomimetics, Vol. 10, No. 4, 2025, p. 208.

[26] X. Zhang, N. Sun, G. Liu, T. Yang, J. Yang, "Disturbance Preview-Based Output Feedback Predictive Control for Pneumatic Artificial Muscle Robot Systems With Hysteresis Compensation", IEEE/ASME Transactions on Mechatronics, Vol. 29, No. 5, 2024, pp. 3936-3948.

[27] V. P. Tran, T. H. T. Nguyen, H. N. Ngo, M. K. Nguyen, C. N. Nguyen, C. N. Nguyen, "Điều khiển vị trí cơ nhân tạo khí nén sử dụng bộ điều khiển PID [Position control of a pneumatic artificial muscle using a PID controller]", Can Tho University Journal of Science, Vol. 59, 2023, pp. 45-49.

[28] J. Takosoglu, "Angular position control system of pneumatic artificial muscles", Open Engineering, Vol. 10, No. 1, 2020, pp. 681-687.

[29] C.-J. J. Lin, T.-Y. Y. Sie, W.-L. L. Chu, H.-T. T. Yau, C.-H. H. Ding, "Tracking Control of Pneumatic Artificial Muscle-Activated Robot Arm Based on Sliding-Mode Control", Actuators, Vol. 10, No. 3, 2021, p. 66.

[30] T. C. Tsai, M. H. Chiang, "Design and control of a 1-DOF robotic lower-limb system driven by novel single pneumatic artificial muscle", Applied Sciences, Vol. 10, No. 1, 2020, p. 43.

[31] Z. Zhou, Y. Lu, S. Kokubu, P. E. Tortós, W. Yu, "A GAN based PID controller for highly adaptive control of a pneumatic-artificial-muscle driven antagonistic joint", Complex & Intelligent Systems, Vol. 10, No. 5, 2024, pp. 6231-6248.

[32] H. Khajehsaeid, A. Soltani, V. Azimirad, "Design of an Adaptive Fixed-Time Fast Terminal Sliding Mode Controller for Multi-Link Robots Actuated by Pneumatic Artificial Muscles", Biomimetics, Vol. 10, No. 1, 2025.

[33] A. M. El-Nagar, A. Abdrabou, M. El-Bardini, E. A. Elsheikh, "Embedded Fuzzy PD Controller for Robot Manipulator", Proceedings of the International Conference on Electronic Engineering, Menouf, Egypt, 3-4 July 2021, pp. 1-6.

[34] I. N. Al-Obaidi, "Design Of Fuzzy-Pd Controller For Heating System Temperature Control", Bilad Alrafidain Journal for Engineering Science and Technology, Vol. 1, No. 1, 2022, pp. 16-20.

[35] S. Dan, H. Cheng, Y. Zhang, H. Liu, "A Fuzzy Indrect Adaptive Robust Control for Upper Extremity Exoskeleton Driven by Pneumatic Artificial Muscle", Proceedings of the IEEE International Conference on Mechatronics and Automation, Guilin, Guangxi, China, 7-10 August 2022, pp. 839-846.

[36] S. W. Chan, J. H. Lilly, D. W. Repperger, J. E. Berlin, "Fuzzy PD+I learning control for a pneumatic muscle", Proceedings of the 12th IEEE International Conference on Fuzzy Systems, St. Louis, MO, USA, 25-28 May 2003, pp. 278-283.

[37] H. Chaudhary, V. Panwar, N. Sukavanum, R. Prasad, "Fuzzy PD+I based Hybrid force/ position control of an Industrial Robot Manipulator", IFAC Proceedings Volumes, Vol. 47, No. 1, 2014, pp. 429-436.

[38] C.-N. Nguyen, C.-N. Nguyen, "Fuzzy Control: A Textbook", Can Tho: Can Tho University Publishing House, 2020.